Analyst

Accepted Manuscript

ROYAL SOCIETY OF CHEMISTRY

www.rsc.org/analyst

The Analyst

RSCPublishing

ARTICLE

Sensing cisplatin-induced permeation of single live human bladder cancer cells by scanning electrochemical microscopy

Meng-Ni Zhang[a,b], Zhifeng Ding[a]*, Yi-Tao Long[b]*

Cite this: DOI: 10.1039/x0xx00000x

Received 00th January 2012,
Accepted 00th January 2012

DOI: 10.1039/x0xx00000x

www.rsc.org/

Cisplatin is a widely used anti-cancer agent, which was believed to trigger apoptosis of cancer cells by forming DNA adducts. However, recent studies evidenced a cisplatin-induced extrinsic apoptotic pathway through the interaction with plasma membranes. We present quantitative time-course imaging of cisplatin-induced permeation of ferrocenemethanol to single live human bladder cancer cells (T24) using scanning electrochemical microscopy (SECM). Simultaneous quantification of cellular topography and membrane permeability was realized by running SECM depth scan mode. It was demonstrated that the acute addition of cisplatin to the outer environment of T24 cells immediately induced membrane permeability change in 5 min, which indicated a loosened structure of the cellular membrane upon the cisplatin dosage. The cisplatin-induced permeation of T24 cell might be a one-step action, an extrinsic mechanism, since the cell response was quick, and no continuous increase in the membrane permeability was observed. Time-lapse SECM depth scan method provided a simple and facile way of monitoring cisplatin-induced membrane permeability changes. Our study is anticipated to lead to a methodology of screening anti-cancer drugs through their interactions with live cells.

Introduction

Bladder cancer is the fourth most common cancer of men and the eighth most common cancer of women, and has unusually high rate of reoccurrence[1]. Like most of other cancers, bladder cancer begins with the mutation of one single cell[2]. Investigations of bladder cancer, especially their interactions with anti-cancer drugs, at the single cell level can provide new insights into physiology, pathology and pharmacology, and promote the development of chemotherapy[3]. Cisplatin is one of the most widely used anti-cancer agents[4-6] and can be used as the single or combination agent in chemotherapy of bladder cancers.[7] People used to believe that cisplatin-induced apoptosis was through the formation of DNA adducts[8-10]. However, the cisplatin-induced side effects suggest the contribution of non-DNA targets to its anti-cancer action and toxicity[11, 12]. Indeed, the DNA-damaging mechanism cannot explain all the cisplatin actions, and several works have recently conducted for its effect on the plasma membranes[11, 13, 14].

The plasma membrane is the first cellular barrier that anti-cancer agents encounter in live cell system. Mounting evidence indicates that cisplatin-induced apoptosis involves the formation of plasma membrane rafts therefore triggers the extrinsic apoptosis pathway[15-17]. In such process cisplatin interacts with membrane proteins, exchangers, channels, and alters the membrane fluidity and permeability[11-14]. Membrane permeability is an important property that presents a measure for the membranes to transport substances via different mechanisms. While the permeability to large, polar molecules or ions presents the function of specific protein channels or transporters[13, 18-20], that to small, non-polar molecules reflects the membrane integrity and structural functions of the membranes[21].

As a non-invasive analysis method[22-27], scanning electrochemical microscopy (SECM) has been successfully applied to studies of the extracellular reactive oxygen and nitrogen species[28-35], and membrane permeability of single live cells, such as the permeability of the nuclear envelope at isolated Xenopus Oocyte nuclei[36], the effect of Triton X-100 on the membrane of HeLa cells[37], the permeability of algal protoplast to different compounds,[38] redox properties at the subcellular level[39], as well as other biophysical studies[40, 41]. In SECM, an ultramicroelectrode (UME) as the probe provides sufficient spatiotemporal resolution to reveal the cell morphology[25-27, 29] and fast kinetics[36, 37, 42, 43] at permeable membranes. Our SECM instrument has a close-loop nature and can repeatedly scan exactly the same area, which enables time-lapse measurements[44]. Here we exploit time-lapse SECM as a rapid, quantitative method to monitor the time-course cisplatin-

induced variation in T24 cell membrane permeability. Conventional SECM method to quantify the membrane permeability is to use probe approach curves (PACs, curves of the probe current current versus its distance to substrates)[36, 37]. However, such measurement is conventionally only for single course that is time consuming and visibility for changing in cellular topography is poor. Especially, when anti-cancer agents such as cisplatin were applied, the cellular topography and membrane permeability were found to change simultaneously. Thus we applied the novel SECM mode, depth imaging, which was recently incorporated into SECM[45]. A batch of PACs can be collected effectively at once and the topographical alteration could be visualized in real time. In addition, time-lapse depth imaging adds advantages in temporal resolution. We chose ferrocenemethanol ($FcCH_2OH$), which is non-cytotoxic[29] and simply diffuses through permeable membranes[38], as probe of T24 membrane permeability.

Materials and Methods

Chemicals

Cisplatin, $FcCH_2OH$, phosphate buffered saline (PBS) were purchased from Sigma-Aldrich (Mississauga, ON). The pH 7.4 PBS solution was prepared with 18 MΩ Milli-Q water (Millipore, Etobicoke, ON), which were used to prepare all other solutions. The concentrations of the cisplatin and $FcCH_2OH$ stock solutions in PBS are 3.00×10^4 ng/mL (0.10 mM) and 1.08×10^5 ng/mL (0.50 mM), respectively.

Cell culture, treatment and preparation

T24 cells were supplied by American Type Culture Collection (ATCC, Manassas, VA). All the culture medium (DMEM), and supplements were purchased from Gibco (Invitrogen, Burlington, ON). T24 cells were incubated in a 37 ℃ incubator for at least 12 h before being brought to SECM experiments. The cultured T24 cells were divided into two groups: control group and cisplatin-challenged group. All cells were washed with pH 7.4 PBS solution for 3 times after culturing and refilled with 3 mL fresh pH 7.4 PBS solution containing 1.08×10^5 ng/mL (0.50 mM) $FcCH_2OH$ prior to SECM experiments. 7.50×10^3 (0.025 mM)ng/mL cisplatin (final concentration) was added directly to the cisplatin-challenged group in SECM experiments. The $FcCH_2OH$ concentration was not diluted upon the addition of the cisplatin since its stock solution contained also 1.08×10^5 ng/mL (0.50 mM) $FcCH_2OH$.

Fabrication of the UMEs

The platinum UMEs with a diameter of 5 μm were prepared by sealing 5 μm Pt wires (Goodfellow Metals, Cambridge, UK) in a tapered end of a glass capillary (o.d.: 2 mm; i.d.: 1 mm; length: 5 cm; Sutter Instrument, Novato, CA) pulled with a heating-coil puller (PP-83, Narishige, Japan). The sealed end was grinded to expose the disk shaped Pt, polished with Al_2O_3 polishing pad (0.05 micron, Buehler, ON) to get a smooth electrode surface, and trimmed down to a RG value of 3.5 (the ratio of the glass radius to the platinum disk radius). The prepared SECM probes were characterized as described elsewhere[46, 47].

SECM instrumentation

The SECM instrument was modified from Alpha-SNOM (Witec, Ulm, Germany) scanning probe microscope by mounting a home-made electrode holder on the objective lens turret. The sophisticated positioning system of the microscope can precisely control the displacement of the UME along x, y and z axes with a minimum displacement of 1 nm. Raster scans can be conducted in both the horizontal (x-y) plane and vertical (x-z) planes as show in Figure 1. All the electrochemical experiments were performed with an electrochemical analyzer (CHI 800b, CH Instruments, Austin, TX), and the current signal was fed into the Alpha-SNOM instrument through a data acquisition channel. The output current signal from the real panel of the CHI 800b workstation equipped with a Picoamp Booster (CHI 200, CH Instruments) was filtered by a custom-made Notch filter to reduce the 60 Hz noise from the main electricity power. Other details of instrumentation and operation procedures of SECM were described by us elsewhere[29].

SECM measurements

In SECM experiments, a Petri dish with T24 cells attached to the bottom was mounted on the heated scanning stage. The temperature of the heating stage (Bioscience Tools, San Diego, CA) was controlled at 37.0 ± 0.2 ℃ throughout the SECM experiments. At the beginning a single T24 cell was located with an inverted microscopic object lens (Nikon, Japan). The UME was immersed into the PBS solution and was biased at 0.400 V vs. Ag/AgCl reference electrode. The oxidation of $FcCH_2OH$ at the diffusion-controlled rate gives a steady state current i_∞ when the UME is far away from the cell, Figure 1A. The current decreases as the UME approached to the selected T24 cell since the membrane in the cell resting stage blocks the diffusion of $FcCH_2OH$ (Figure 1B)[29, 46-48]. The position of the UME at this height was marked as z = 0 μm. For the control cell group, time-lapse SECM depth scans were conducted repeatedly for 1 hour within a vertical (x-z) plane, where z was set from 20 to 0 μm and x from 0 to 40 μm. It took 3 min for each depth image of the above geometry in 128 pixels by 128 pixels. 12 SECM depth-scan images were obtained with an interval of 5 min. For the cisplatin-challenged cell group, one depth scan image was taken firstly without cisplatin. Cisplatin was added once the SECM depth scan was over. 2 min later, time-lapse SECM scans were performed for 1 h with the same 5 min time interval, Figure 1C. Experimental PACs were extracted from these time-lapse depth scan images by drawing vertical lines at specific points.

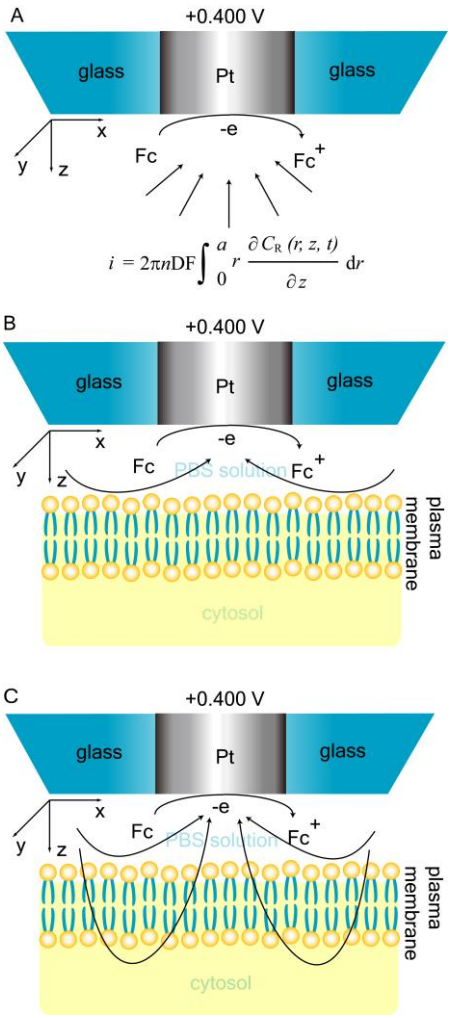

Figure 1. Principle of measuring membrane permeability by SECM with ferrocenemethanol as the probe. (A) Hemispherical diffusion of ferrocenemethanol to the UME surface in the bulk solution. (B) The flux of ferrocenemethanol is blocked by a live cell in resting stage. (C) Ferrocenemethanol diffuses across permeable membranes thus the flux is higher than that of cells in resting stage.

Results and discussion

Simulation of the membrane permeability of T24 cells by SECM

In this section we present our simulations of the membrane permeability, P_m, using the model described in Electronic Supplementary Information. Theoretical SECM PACs with different P_m values (Figure 2) were simulated by assuming the center symmetry and running finite elemental analysis in 2D axial symmetry (See ESI). Figure 2 demonstrates also the PACs depending on the permeability of the membrane in the range of 0.0 to 1.0×10^{-3} m/s. If a vertical line is drawn across all the PACs in Figure 2 at a normalized distance of 1, the current increases upon augmentation of the permeability. This is reasonable since the inward and outward fluxes of the cell were both increased. Noticeably, PACs with $P_m \leq 1.0 \times 10^{-7}$ m/s and P_m = 0.0 m/s overlap together and cannot be distinguished. Step-by-step instruction of programming simulation with COMSOL software (v3.5a) is described in ESI and an example code is available upon request to the authors.

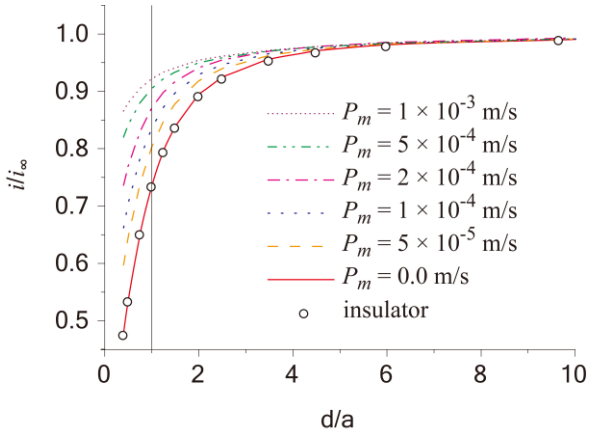

Figure 2. Theoretical PACs from an insulator (open circles), and cells with membrane permeability coefficient P_m = 1.0×10^{-3} m/s, 5.0×10^{-4} m/s, 2.0×10^{-4} m/s, 1.0×10^{-4} m/s, 5.0×10^{-5} m/s, and 0.0 m/s (solid curves from top to bottom).

When the UME was placed in the close proximity of a cell in resting stage that is similar to an insulator (Figure 2), the flux of $FcCH_2OH$ to the UME surface was blocked (Figure 1B). Thus the current was smaller than i_∞. As the UME kept approaching to the cell, the current remained decreasing, which is called negative feedback in SECM. When the UME was in the close proximity of a live cell that was somehow permeable to $FcCH_2OH$ (for instance, $P_m = 1.0 \times 10^{-3}$ m/s (Figure 1C)), such permeabilization added an extra flux of $FcCH_2OH$ to the UME. The PAC (top curve in Figure 2) show less negative feedback than the one to the cell in resting stage. It should be noticed that the PACs to a cell with $P_m \leq 1.0 \times 10^{-7}$ m/s overlap with that to an insulator (pure negative feedback), meaning that membranes with $P_m \leq 1.0 \times 10^{-7}$ m/s are in the resting stage and nearly impermeable. Different membrane permeability can be distinguished and determined quantitatively by fitting the experimental PACs to the theoretical ones.

The above observations agree very well with those obtained by Matsue's group[38], who investigated permeation of redox species through a single, living algal protoplast.

SECM depth scan images and probe approach curves

SECM depth scan mode was adapted from that of confocal microscopy[31, 45]. Figure 3 illustrates time-lapse SECM depth scan images at 0 min (Figure 3A) and 45 min (Figure 3B). As the T24 cell blocks $FcCH_2OH$ molecules from diffusing to the UME surface, a typical mirror dark hemisphere SECM image of the T24 cell can be observed.

PACs can be extracted from any position of the SECM depth scan images by drawing vertical lines toward spots of interest on images. Figure 3C demonstrates original experimental PACs to the centre of the cell, which seemed to present different P_m at 0 min and 45 min. Noticeably, there is a gap between the two PACs represented by a displacement in z direction.

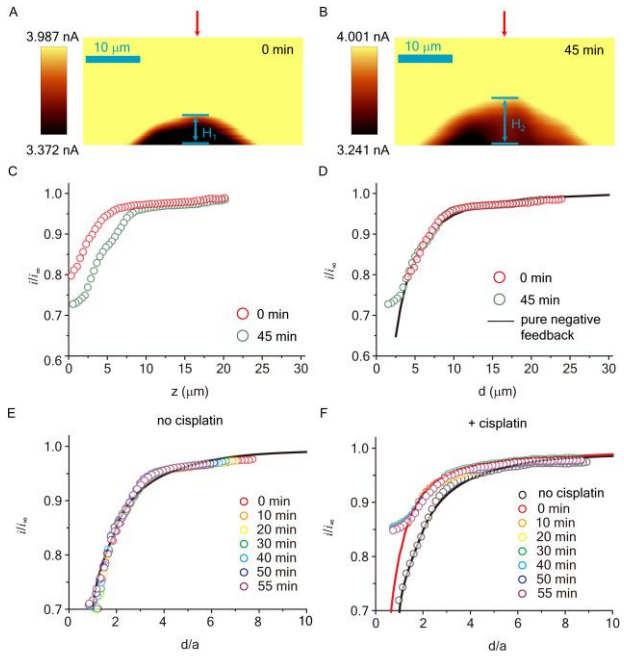

Figure 3. (A) & (B): Time-lapse SECM depth scan images of a control T24 cell. (C) Experimental PACs from the red arrow pointed position . (D) Experimental PACs fitted to a theoretical PAC. d: probe-to-cell distance. (E) & (F) Adjusted time-lapse PACs. Solid lines: Theoretical PACs of $P_m \leq 1.0 \times 10^{-7}$ m/s (black), $P_m = 5.0 \times 10^{-5}$ m/s (red).

The distance gap between two experimental PACs (Figure 3C) might be caused by increased cellular topography. The real probe-to-cell distance at the bottom of the SECM depth scan images was obtained by fitting the experimental PACs to the theoretical PAC representing pure negative feedback approximately (Figure 3D). According to Figure 3D, at 0 min, the probe-to-cell distance at the bottom of Figure 3A was 3.87 μm in the assumption of negative feedback, while at 45 min, the probe-to-cell distance at the bottom of Figure 3B was ca. 1.08 μm. In time-lapse SECM depth scans, the UME scans over the same area repeatedly, therefore the decreased probe-to-cell distance at the bottom of the time-lapse SECM depth scan images indicates about 2.79 μm increase in the cellular height. We noticed that within 45 min, the dark hemisphere corresponding to the T24 cell in the SECM depth scan images had expanded. We took the point where $i = 0.9\ i_\infty$ on the central vertical line as the top edge of the dark hemisphere and measured the height of the dark hemisphere in both Figure 3A (H_1) and Figure 3B (H_2) for comparison. The increase of the height of the dark hemisphere in Figure 3A and Figure 3B was determined to be $H_2 - H_1 = 2.67$ μm, which is in good agreement with the distance gap between the time-lapse PACs in Figure 3C.

In SECM, the feedback effect always depends on the probe-to-cell distance[49]. At t = 0 min, the current decreased to $i = 0.9i_\infty$ when the probe-to-cell distance reached d_1 (Figure 4). 45 min later, the UME still need to approach the cell till the probe-to-cell distance equals to d_1 to obtain current $i = 0.9i_\infty$. However, as the cellular topography had increased by Δh, the point where $i = 0.9i_\infty$ will accordingly move upward by Δh in the SECM depth scan image (Figure 4). Therefore, the alteration in the height of the dark hemisphere in time-lapse SECM images represented the actual change in the cellular height. Due to such advantage of SECM depth scans, the experimental PACs can be adjusted along z axis according to the visualized topographical alteration, therefore the actual variation in the curvature of PACs can be revealed. After such adjustment, the time-lapse experimental PACs from every control cell overlap together (Figure 3E), indicating that the membrane permeability did not change within the SECM experiment duration. For each cisplatin-challenged cell, the time-lapse PACs after cisplatin addition have the same curvature; however they present less negative feedback than the PAC before cisplatin addition (Figure 3F).

In conventional time-lapse SECM PAC experiments, the UME was held at a certain height at the beginning, then moves down for a certain distance along z axis. The current was recorded as a function of the displacement in z direction to plot a PAC. After one PAC, the UME was brought to its original position to start another PAC over the same distance along z axis. Such method is time consuming and visualization for change in cellular topography of live cells is poor. Our SECM depth scan mode incorporated information on cell topography and reactivity. In this way, the cell height in real time, and the time-lapse PACs can be visually distinguished by comparing depth scan images which are essential in SECM studies of membrane permeability.

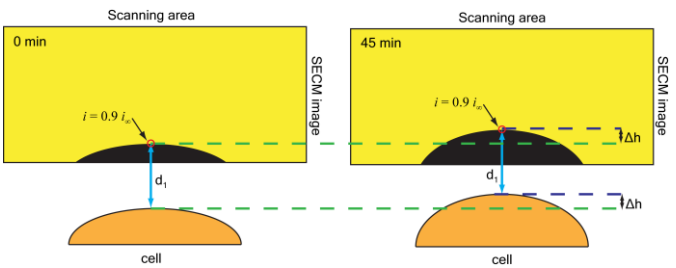

Figure 4. Correlation between the increase in the negative feedback area in SECM depth scan images and the increase in cellular topography. Open circle: the point where $i = 0.9i_\infty$.

Time course of the cisplatin effect on the membrane permeability

In order to monitor the cisplatin-induced variation of the membrane permeability in real time, 7.50×10^3 ng/mL (0.025 mM) cisplatin (final concentration) was added *in situ* for the SECM experiment. This dosage is mimicking chemotherapy of acute bladder exposure to cisplatin as the single agent. The time-lapse SECM depth scans were conducted for 60 min at a time interval of 5 min to record the time-course cisplatin effect on the membrane permeability. The electrochemical reactivity of cisplatin was confirmed by cyclic voltammetry (CV). Figure 5 shows the cyclic voltammogram of 1.50×10^4 ng/mL (0.050 mM) cisplatin in 7.46×10^6 ng/mL (0.1 M) KCl electrolyte solution. Cisplatin does not show electrochemical reactivity until 0.620 V vs. Ag/AgCl. The CV result confirmed that the

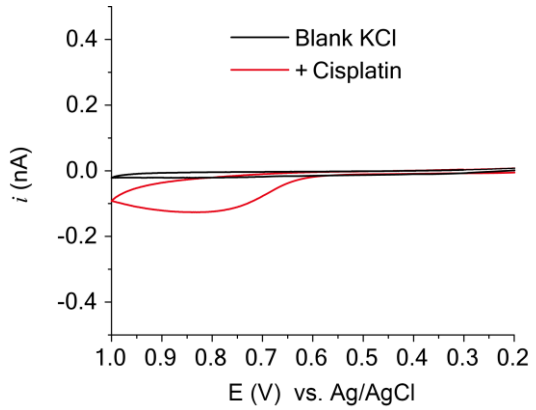

Figure 5. Cyclic voltammograms of 1.50×10^4 ng/mL (0.050 mM) cisplatin in 7.46×10^6 ng/mL (0.1 M) KCl electrolyte solution (red) and 7.46×10^6 ng/mL (0.1 M) KCl blank electrolyte solution (black).

cisplatin is not electrochemically active at 0.400 V vs. Ag/AgCl at which FcCH2OH is oxidized. Therefore no current resulting from cisplatin was involved in our SECM experiments. The adjusted time-lapse PACs to a control T24 cell (Figure 3E) and a cisplatin-challenged T24 cell (Figure 3F) are compared. The adjusted time-lapse PACs to the control T24 cell present the same curvature, indicating constant membrane permeability within the SECM experiment duration (Figure 3E). While the adjusted time-lapse PACs to the cisplatin-challenged T24 cell present the same curvature (color curves in Figure 3F), it shows more positive feedback than that before the cisplatin addition (black curve in Figure 3F). As observed from the theoretical PACs presenting different membrane permeability (Figure 2), after adding cisplatin, this tendency toward more positive feedback rationales an increase in the membrane permeability for the cisplatin-challenged T24 cell. The cell reacted to the cisplatin dosage in 5 min, and did not change any further over time. The same result was obtained with 3 parallel experiments.

In order to examine if cisplatin alters the membrane permeability to the same extent with every T24 cell, or the change varies from cell to cell, the average time-lapse current of three control T24 cells and three cisplatin-challenged T24 cells at the same probe-to-cell distance (z/a = 1.5, setting the bottom of the first SECM depth scan image of each image set as z = 0) was read from the experimental time-lapse PACs in a time course of 60 min. Figure 6 demonstrate the average current values versus time in the SECM experimental duration, where error bars show deviations from the average values. Without cisplatin treatment (empty bars in Figure 6), the average normalized current over control cells at the constant probe-to-cell distance does not change with time. The maximum standard deviation is 6.8×10^{-3} in Figure 6, suggesting that the membrane permeability of the control T24 cells to $FcCH_2OH$ does not differ from cell to cell over the time. Once cisplatin was administrated to the T24 cells (filled bars in Figure 6), the electrochemical current at the constant probe-to-cell distance immediately (within 5 min) increased to a higher level, and remained at that level without further changing with time. Since the detected current is proportional to the flux of $FcCH_2OH$, the elevated current level is attributed to the cisplatin-induced permealization of the plasma membrane of T24 cells. The maximum standard deviation in Figure 6 is 9.2×10^{-3}, indicating that cisplatin induced similar alteration in the membrane permeability for every T24 cell over the time course. To quantitatively elucidate the cisplatin effect on the membrane permeability of T24 cells, we only need to determine two parameters, that is, the membrane permeability without cisplatin treatment and the membrane permeability under cisplatin treatment.

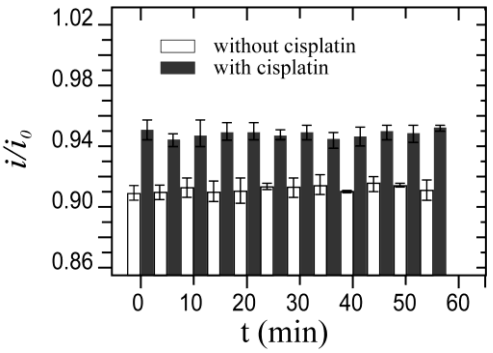

Figure 6. Time-lapse average probe current at z/a = 1.5 (z is the displacement of the UME during depth imaging. At the bottom of the first depth scan image in an image set, z = 0) from (A) three control T24 cells and (B) cisplatin-challenged T24 cells. Error bars show the deviations from the average values.

Quantification of the cisplatin effect on the membrane permeability of T24 cells

The membrane permeability of control T24 cells and cisplatin-challenged T24 cells was determined by overlaping the experimental PACs to the theoretical ones. Figure 3E and Figure 3F show an example of three parallel fittings under each condition. The experimental PACs to a control T24 cell overlaps with the theoretical PAC, leading to a $Pm \leq 1.0 \times 10^{-7}$ m/s, which means a T24 cell in the resting stage is nearly impermeable to ferrocenemethanol. In the same manner, the experimental PACs over a cisplatin-challenged T24 cell superposes to the theoretical PAC with $Pm = 5.0 \times 10^{-5}$ m/s. According to these two values, we can conclude that cisplatin treatment efficiently permeabilized T24 cells in 5 min, which increased the permeability coefficient to ferrocenemethanol from $\leq 1.0 \times 10^{-7}$ m/s to 5.0×10^{-5} m/s.

Qualitatively, similar time-lapse membrane permeability behaviour was observed with each group of T24 cells. The addition of cisplatin quickly increases (within 5 min) and maintains the membrane permeability of the T24 cells. Cisplatin effect on the plasma membranes of cancer cells was recently considered as an extrinsic pathway of apoptosis[11, 17] which involves membrane fluidification and permeabilization[11, 12, 14]. The cisplatin-induced permeation of T24 cells probed by $FcCH_2OH$ here agrees well with those observations, indicating a loosened structure of the plasma membrane. It was reported that the cisplatin-induced permeation of plasma membrane leads to an enhanced cisplatin uptake [12]. Therefore a continuous

increase in the membrane permeability was expected with the enhanced cisplatin uptake is expected if the cisplatin-induced permeation is an intracellular controlled process. However, the cisplatin-induced permeation of the cellular membrane of T24 cells observed here is a one-step action, and no continuous increase in the membrane permeability was observed in our experimental time scale. This might implicate an extracellular mechanism in which the cisplatin-induced permeation is controlled by the direct contact between cisplatin and the plasma membrane.

Table 1. Permeability of different bio-membranes.

[a] membrane permeability to ferrocenemethanol. [b] membrane permeability to ferrocyanide.

Membrane type	Permeability (10^{-5} m/s)
[a]Human bladder cancer cells' plasma membrane	5.0
[a]Frog egg's nuclear envelope [36]	740
[b]HeLa cells' plasma membrane [37]	0.65
[a]Algal cells without cell walls [38]	5.0

Quantitatively, upon the addition of 0.0080 mg/mL (0.027 mM) cisplatin, the membranes permeability coefficient of T24 cells increased from $\leq 1.0 \times 10^{-7}$ m/s to 5.0×10^{-5} m/s in 5 min. The effectiveness of cisplatin on the plasma membrane of T24 cell was quantitatively revealed by time-lapse SECM depth scan simply by fitting an experimental PAC obtained in 3 min to theoretical ones.

The permeability of different bio-membranes studied by other groups[36-38] and this work is listed in Table 1. Membrane permeability of cisplatin-challenged T24 cells is very similar to that of algal protoplast (plant cells without cell walls). A major difference between plasma membrane of plant cells and mammalian cells is the cholesterol content[50]. While mammalian cells contain high level of cholesterol in the plasma membrane, there is little cholesterol in the plasma membrane of plant cells[50]. High cholesterol content in the plasma membrane of mammalian cells results in less defects in the bilayer structure of plasma membrane and a decreased permeability to small neutral molecules[51]. After cisplatin addition, the membrane permeability of T24 cells altered to the same level as plasma membrane of plant cells, which has little cholesterol thus has much looser structure. This comparison indicates the effectiveness of the cisplatin on loosening the structure of plasma membrane of T24 cells.

Conclusions

We successfully revealed the cisplatin-induced permeation of intact T24 cells by a novel SECM technique, time-lapse SECM depth scan. This technique allows us to obtain probe approach curves while monitoring the variation of the cell topography in real time. The collection of experimental PACs can be conducted continuously for a long time since the cell remains intact and alive in SECM experiments, therefore enables real-time monitoring of the cellular response upon exogenous stimuli. High temporal resolution combined with non-invasive nature renders time-lapse SECM depth scan a promising method to quantitatively investigate the effectiveness, kinetics and mechanism of anti-cancer drugs basing on responses of single live cells in real time. Membrane permeability might be used as a measure to screen anti-cancer drugs and probe for comprehensive understanding of pathology and pharmacology in chemotherapeutics.

Acknowledgements

This work is supported by NSERC, CIPI, OPC, CFI, OIT, PREA, UWO (ZD), NSFC (YTL, 21327807) and CSC scholarship (MZ). We also thank Prof. Allen J Bard, Dr. Renaud Cornut for helps in simulation modelling, and John Vanstone, Jon Aukema, Sherrie McPhee, Marylou Hart for their quality technical support.

Notes and references

[a] Department of Chemistry, the University of Western Ontario, London, ON, Canada N6A 5B7.

[b] Key Laboratory for Advanced Materials & Department of Chemistry, East China University of Science & Technology, Shanghai, China 200237.

* Corresponding authors:

Zhifeng Ding: Tel.: +1 519 661 2111x86161; fax: +1 519 661 3022; E-mail address: zfding@uwo.ca; URL: http://publish.uwo.ca/~zfding

Yi-Tao Long: Tel.: +86 21 64252339; fax: +86 21 64250032; E-mail address: ytlong@ecust.edu.cn

Running head: SECM of cancer-drug and cell interactions.

† Electronic Supplementary Information (ESI) available for detailed COMSOL simulations. See DOI: 10.1039/b000000x/

1. A. M. Kamat and D. L. Lamm, *J. Urology*, 1999, **161**, 1748-1760.
2. R. Weinberg, *One Renegade Cell: The Quest For The Origin Of Cancer*, Basic Books, New York, 1999.
3. R. H. Templer and O. Ces, *J. Roy. Soc. Interface*, 2008, **5**, S111-S112.
4. J. C. Dabrowiak, *Metals in Medicine*, Wiley, Hoboken, 2009.
5. J. Peng, R. Mandal, M. Sawyer and X.-F. Li, *Clin. Chem.*, 2005, **51**, 2274-2281.
6. C. M. Sturgeon, M. J. Duffy, U.-H. Stenman, H. Lilja, N. Brunner, D. W. Chan, R. Babaian, R. C. Bast, Jr., B. Dowell, F. J. Esteva, C. Haglund, N. Harbeck, D. F. Hayes, M. Holten-Andersen, G. G. Klee, R. Lamerz, L. H. Looijenga, R. Molina, H. J. Nielsen, H. Rittenhouse, A. Semjonow, I.-M.

Shih, P. Sibley, G. Soletormos, C. Stephan, L. Sokoll, B. R. Hoffman and E. P. Diamandis, *Clin. Chem.*, 2008, **54**, e11-79.
7. N. Ismaili, M. Amzerin and A. Flechon, *J. Hematol. Oncol.*, 2011, **4**, 35.
8. R. J. Knox, F. Friedlos, D. A. Lydall and J. J. Roberts, *Cancer Res.*, 1986, **46**, 1972-1979.
9. S. J. Lippard, *Pure Appl. Chem.*, 1987, **59**, 731-742.
10. S. E. Sherman and S. J. Lippard, *Chem. Rev.*, 1987, **87**, 1153-1181.
11. A. Rebillard, D. Lagadic-Gossmann and M.-T. Dimanche-Boitrel, *Curr. Med. Chem.*, 2008, **15**, 2656-2663.
12. K. Wang, J. Lu and R. Li, *Coordin. Chem. Rev.*, 1996, **151**, 53-88.
13. N. Milosavljevic, C. Duranton, N. Djerbi, P. H. Puech, P. Gounon, D. Lagadic-Gossmann, M. T. Dimanche-Boitrel, C. Rauch, M. Tauc, L. Counillon and M. Poët, *Cancer Res.*, 2010, **70**, 7514-7522.
14. A. Rebillard, X. Tekpli, O. Meurette, O. Sergent, G. LeMoigne-Muller, L. Vernhet, M. Gorria, M. Chevanne, M. Christmann, B. Kaina, L. Counillon, E. Gulbins, D. Lagadic-Gossmann and M.-T. Dimanche-Boitrel, *Cancer Res.*, 2007, **67**, 7865-7874.
15. S. Lacour, A. Hammann, S. Grazide, D. Lagadic-Gossmann, A. Athias, O. Sergent, G. Laurent, P. Gambert, E. Solary and M.-T. Dimanche-Boitrel, *Cancer Res.*, 2004, **64**, 3593-3598.
16. C.-R. Huang, Z.-X. Jin, L. Dong, X.-P. Tong, S. Yue, T. Kawanami, T. Sawaki, T. Sakai, M. Miki, H. Iwao, A. Nakajima, Y. Masaki, Y. Fukushima, M. Tanaka, Y. Fujita, H. Nakajima, T. Okazaki and H. Umehara, *Anticancer Res.*, 2010, **30**, 2065-2071.
17. O. Vondálová Blanářová, I. Jelínková, Á. Szöőr, B. Skender, K. Souček, V. Horváth, A. Vaculová, L. Anděra, P. Sova, J. Szöllősi, J. Hofmanová, G. Vereb and A. Kozubík, *Carcinogenesis*, 2011, **32**, 42-51.
18. H. Sato, H. Hakamada, Y. Yamazaki, M. Uto, M. Sugawara and Y. Umezawa, *Biosens. Bioelectron.*, 1998, **13**, 1035-1046.
19. G. Ghosh, I. Mehta, A. L. Cornette and K. W. Anderson, *Biosens. Bioelectron.*, 2008, **23**, 1109-1116.
20. Z. Chen, S. Xie, L. Shen, Y. Du, S. He, Q. Li, Z. Liang, X. Meng, B. Li, X. Xu, H. Ma, Y. Huang and Y. Shao, *Analyst*, 2008, **133**, 1221-1228.
21. B. Alberts, *Molecular biology of the cell: Reference edition*, Garland Science, New York, 2008.
22. I. Beaulieu, S. Kuss, J. Mauzeroll and M. Geissler, *Anal. Chem.*, 2011, **83**, 1485-1492.
23. B. Liu, S. A. Rotenberg and M. V. Mirkin, *Proc. Natl. Acad. Sci. USA*, 2000, **97**, 9855-9860.
24. A. Schulte and W. Schuhmann, *Angew. Chem., Int. Edit.*, 2007, **46**, 8760-8777.
25. A. J. Bard, X. Li and W. Zhan, *Biosens. Bioelectron.*, 2006, **22**, 461-472.
26. S. Amemiya, J. Guo, H. Xiong and D. Gross, *Anal. Bioanal. Chem.*, 2006, **386**, 458-471.
27. X. Zhao, P. M. Diakowski and Z. Ding, *Anal. Chem.*, 2010, **82**, 8371-8373.
28. S. E. Salamifar and R. Y. Lai, *Anal. Chem.*, 2013, **85**, 9417-9421.
29. X. Zhao, N. O. Petersen and Z. Ding, *Can. J. Chem.*, 2007, **85**, 175-183.
30. X. Zhao, M. Zhang, Y. Long and Z. Ding, *Can. J. Chem.*, 2010, **88**, 569-576.
31. M. M. N. Zhang, Y.-T. Long and Z. Ding, *J. Inorg. Biochem.*, 2012, **108**, 115-122.
32. C. Amatore, S. Arbault, C. Bouton, K. Coffi, J. Drapier, H. Ghandour and Y. Tong, *ChemBioChem*, 2006, **7**, 653-661.
33. C. Amatore, S. Arbault and M. Erard, *Anal. Chem.*, 2008, **80**, 9635-9641.
34. C. Amatore, S. Arbault, M. Guille and F. Lemaître, *Chem. Rev.*, 2008, **108**, 2585-2621.
35. Y. Wang, J.-M. Noël, J. Velmurugan, W. Nogala, M. V. Mirkin, C. Lu, M. Guille Collignon, F. Lemaître and C. Amatore, *Proc. Natl. Acad. Sci. USA*, 2012, **109**, 11534-11539.
36. J. Guo and S. Amemiya, *Anal. Chem.*, 2005, **77**, 2147-2156.
37. D. Koley and A. J. Bard, *Proc. Natl. Acad. Sci. USA*, 2010, **107**, 16783-16787.
38. T. Yasukawa, I. Uchida and T. Matsue, *BBA - Biomembranes*, 1998, **1369**, 152-158.
39. P. Sun, F. O. Laforge, T. P. Abeyweera, S. A. Rotenberg, J. Carpino and M. V. Mirkin, *Proc. Natl. Acad. Sci. USA*, 2008, **105**, 443-448.
40. M. A. Edwards, S. Martin, A. L. Whitworth, J. V. Macpherson and P. R. Unwin, *Physiol. Meas.*, 2006, **27**, R63.
41. Y. Takahashi, A. I. Shevchuk, P. Novak, B. Babakinejad, J. Macpherson, P. R. Unwin, H. Shiku, J. Gorelik, D. Klenerman, Y. E. Korchev and T. Matsue, *Proc. Natl. Acad. Sci. USA*, 2012, **109**, 11540-11545.
42. K. McKelvey, M. E. Snowden, M. Peruffo and P. R. Unwin, *Anal. Chem.*, 2011, **83**, 6447-6454.
43. R. Ishimatsu, J. Kim, P. Jing, C. C. Striemer, D. Z. Fang, P. M. Fauchet, J. L. McGrath and S. Amemiya, *Anal. Chem.*, 2010, **82**, 7127-7134.
44. X. Zhao, S. Lam, J. Jass and Z. Ding, *Electrochem. Comm.*, 2010, **12**, 773-776.
45. M. S. M. Li, F. P. Filice and Z. Ding, *J. Inorg. Biochem.*, 2014, **136**, 177-183.
46. A. J. Bard, F. R. F. Fan, J. Kwak and O. Lev, *Anal. Chem.*, 1989, **61**, 132-138.
47. R. Zhu and Z. Ding, *Can. J. Chem.*, 2005, **83**, 1779-1791.
48. J. Kwak and A. J. Bard, *Anal. Chem.*, 1989, **61**, 1221-1227.
49. A. J. Bard and M. V. Mirkin, *Scanning Electrochemical Microscopy*, Mercel Dekker, New York, 2001.
50. J. M. Berg, J. L. Tymoczko and L. Stryer, *Biochemistry, 5th edition*, W H Freeman, New York, 2002.
51. P. L. Yeagle, *BBA - Rev. Biomembranes*, 1985, **822**, 267-287.